IEEE Access
Multidisciplinary | Rapid Review | Open Access Journal

Received December 13, 2018, accepted December 19, 2018, date of publication December 27, 2018,
date of current version January 16, 2019.

Digital Object Identifier 10.1109/ACCESS.2018.2889991

Passive Earth Pressures on Retaining Walls for Pit-in-Pit Excavations

HUI HU[1], MENGQI YANG[2], PEIYUAN LIN[3], and XINGLI LIN[4]
[1]School of Mechanics and Construction Engineering, Jinan University, Guangzhou 510632, China
[2]School of Geographical Science, Guangzhou University, Guangzhou 510006, China
[3]Ryerson Institute of Infrastructure Innovation and Department of Civil Engineering, Ryerson University, Toronto, ON M5B 2K3, Canada
[4]Guangzhou Hannan Engineering Technology Co., Ltd., Guangzhou 510411, China

Corresponding author: Peiyuan Lin (peiyuan.lin@ryerson.ca)

This work was supported in part by the National Natural Science Foundation of China under Grant 41472279 and in part by the Provincial Key Technologies R&D Program of Guangdong (No. 32406027).

ABSTRACT The technique of pit-in-pit excavations is increasingly used in China to provide an efficient solution of maximizing the utilization of underground space while minimizing the amount of solid waste due to excavations. One of the critical steps toward the successful implementation of the pit-in-pit excavation technique is to rationally estimate the passive earth pressure, which is typically done using approaches such as numerical modeling, field monitoring, or traditional Coulomb or Rankine earth pressure theories. This paper presents a simplified approach for computing passive earth pressures for pit-in-pit excavations. A trapezoidal-shaped failure wedge is formed between two levels of retaining walls. A complete symmetric soil arch is used to describe the stress field of soils in the rectangular zone, whereas a half arch with one base acting on the wall and another base acting on the inclined shear surface is proposed for soils in the triangular zone. The soil arching effect is explicitly considered to derive the earth pressure for both cohesionless and cohesive soils at any intermediate passive state. A parametric study is conducted to demonstrate that the mobilized passive earth pressure increases nonlinearly with the magnitude of wall movement and soil shear strength parameters. The allowable spacing between two walls is also defined to produce a design chart. In the end, the proposed model is assessed against experimental measurements from model-scale tests.

INDEX TERMS Pit-in-pit excavation, passive earth pressure, retaining wall, analytical solution, wall movement, soil arching.

I. INTRODUCTION

Over the past couple of decades, researchers have worked extensively on the evaluation of lateral earth pressures acting on retaining walls. This is because the development of earth pressures is highly correlated with the magnitude and the mode of mobilized wall movement. The displacement dependency of earth pressures has been reported from field measurements for various geological conditions, including confined backfills against tall rigid walls [1], open cuts in jointed rock mass on a support system [2], pit-in-pit excavations over a large area [3], and the loss of foundation soils due to dewatering [4]. However, field data are influenced by different sources of uncertainty, such as variations in soil properties, temperature, and profiles of soil moisture. Hence, the trends of field data are often hidden, which cannot be used to calibrate analytical solutions directly.

Alternatively, laboratory experiments can be conducted under controlled conditions. Reduced-scale model tests have been performed in a centrifuge environment, where the soil- wall interaction system is subjected to an elevated acceleration field to simulate the stress field at the prototypes-scale. For example, Frydman and Keissar [5] measured the variation of lateral earth pressures on a rigid retaining wall near rock face induced by the rotation of the wall about the base. Take and Valsangkar [6] conducted a series of centrifuge tests to measure earth pressures behind unyielding retaining walls of narrow backfill width using innovative flexible subminiature pressure cells. Hong and Ng [7] studied the base stability of multi-propped excavation and measured the associated ground settlement outside the excavation using centrifuge modelling. A centrifuge facility is not always affordable. Hence, researchers tend to model the behaviour of retaining walls in the 1 g environment following the law of similitude. Fang *et al.* [8] investigated the influence of the mode of wall movement on the mobilization of passive earth pressures against a rigid wall. Fang *et al.* [9] measured the

earth pressures against a vertical rigid wall, and found that the conventional solutions based on Coulomb and Terzaghi theories could overestimate the passive thrust significantly. Recently, Zheng *et al.* [10] conducted a series of model tests to evaluate the performance of pit-in-pit excavations.

Numerical simulation becomes increasingly popular with the advancement of computing capability [11]–[13]. It should be noted that the use of numerical modelling requires engineers to develop expertise and confidence in model calibration. Therefore, design practice is still heavily dependent on analytical solutions. Following the pioneering work of Coulomb, Rankine and Terzaghi, Handy [14] initially introduced the concept of soil arching in the calculation of lateral earth pressures against retaining walls, where the soil prism was divided into strip elements to take into account the nonlinear distribution of earth pressures. Hou [15] extended the Handy arching model and proposed an earth pressure model based on depth-dependent vertical stress above the soil element. Similarly, Qin *et al.* [16] proposed to use a parabolic distributed shape to describe the pattern of vertical stress in the soil prism. Other researchers employed different arch models in the calculation of lateral earth pressures, such as the modified Marston theory [17], the modified Janssen's arch model [18], and the modified Protodyakonov's arch model [19]. Alternatively, the limit equilibrium method has been used by researchers to estimate the earth pressures on a rigid retaining wall, such as the variational technique [20], and the principle of optimality [21]. Various forms of solutions based on the slip line theory has been derived to search the failure pattern behind retaining walls with the least safety, and to calculate the relation between wall movement and passive resistance [22]–[24]. Mei *et al.* [25] initially proposed a displacement-dependent earth pressure model to characterize the correlation between the mobilized earth pressure and soil displacement using an S-shaped function. The model was further extended to analyze the response of retaining walls with geofoam inclusions [26], pile driving induced ground heave [27], and laterally loaded piles [28]. Keshavarz and Ebrahimi [29] derived the passive earth pressures for axisymmetric retaining walls using the Stress Characteristics Method (SCM).

The increasing demand for underground space in congested urban areas in China drives engineers to use pit-in-pit excavations. This is because the excavation area is normally very large, where introducing horizontal struts becomes uneconomic. Some projects require a further excavation with a smaller size to a greater depth. If the size of two levels of excavations does not change, it will be expensive, resulting in a large amount of solid waste due to additional excavation. Hence, the concept of pit-in-pit excavations is developed, where a 2nd level narrow-and-deep excavation is implemented within a 1st level wide-and-shallow excavation. Fig. 1 shows the schematic view of a pit-in-pit excavation. Some case histories have been reported in China [3], [30]. However, there is no proper design method for pit-in-pit excavations, and field cases are often carried out by a trial and error procedure. Researchers used model-scale tests [10] and numerical simulations [13], [30] to provide preliminary guidance for design. Alternatively, beam-on-spring analysis is used in design [31], [32], but the accuracy of the analysis is heavily influenced by the choice of soil reaction models [33].

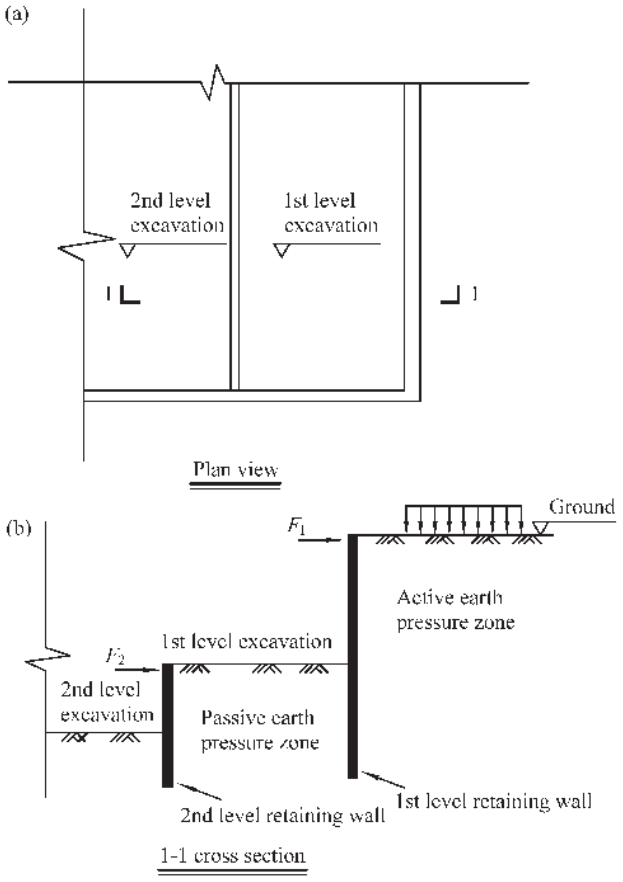

FIGURE 1. Schematics of pit-in-pit braced excavations: (a) plane view; and (b) 1-1 cross section.

The design optimization of safety benches for surface quarries [34] could potentially be modified for use to analyze pit-in-pit excavations. The only work of analytical solution for pit-in-pit excavations is derived by Hu *et al.* [35], where the soil arching effect between two parallel retaining walls is briefly considered. However, the solution of Hu *et al.* [35] can only be used to calculate earth pressures of cohesionless soils at the full passive state. The present paper is an extension of the work by Hu *et al.* [35] to cover cases for both cohesionless and cohesive soils and full and intermediate passive states.

Literature review shows that soil arching effect, and theories of full and intermediate earth pressures have been extensively investigated, while the investigations were isolated in most cases. In this paper, we assembly these isolated components into one analytical framework which can be used to analyze the variation of earth pressures acting on retaining walls for pit-in-pit excavations from intermediate (the state between passive and at-rest) to full passive states for both

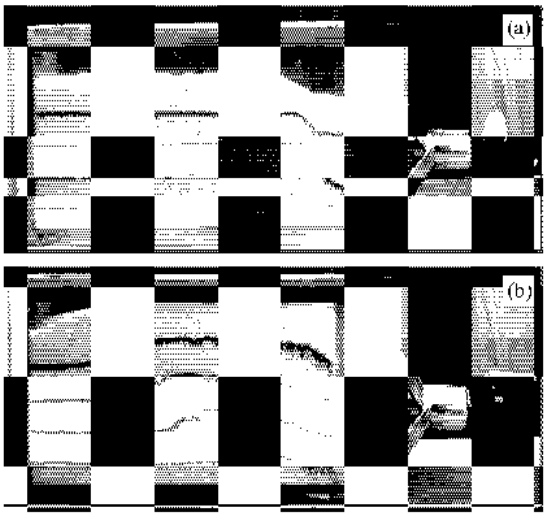

FIGURE 2. Soil arching effect due to (a) active earth pressure mobilized by moving the retaining wall away from the retained soil; and (b) passive pressure mobilized by pushing the retaining wall into the retained soil.

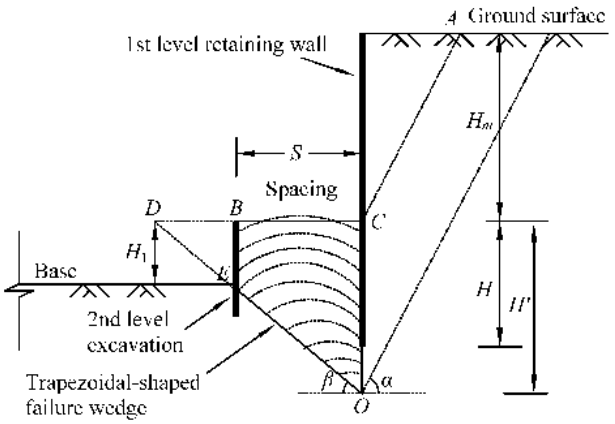

FIGURE 3. Development of soil arching between two retaining walls for pit-in-pit braced excavations.

cohesionless and cohesive soils. A parametric study is then conducted to illustrate how the performance of retaining walls is influenced by pit geometries and soil shear strength parameters. In the end, the efficacy of the proposed analytical model is assessed by comparing calculated earth pressures with those measured in the model-scale tests of Zheng *et al.* [10].

The rest of the paper is structured as follows. Section II discusses theoretical background of this work and presents some preliminary analyses of soil arching effect, full and intermediate passive states of two types of soils. Section III derives analytical solutions for computation of soil passive earth pressure at full and intermediate states taking into account the soil arching effects. The developed closed-form solutions are then validated in Section IV by comparing the predictions to experimental measurements. The paper is concluded in Section V.

II. BACKGROUND AND PRELIMINARIES

The soil arching effect and mobilization of passive state are two key factors for determination of passive earth pressures. Both are not considered in traditional Coulomb and Rankine earth pressure theories. In this section, the theoretical basis of soil arching effect is first introduced, followed by derivations of passive earth pressures at full and intermediate states. The earth pressures at different states are then compared to Coulomb and Rankine theories which are for passive earth pressures at full state.

A. SOIL ARCHING EFFECT

When a retaining wall moves away from the retained soil, the soil near the wall will drop to fill the gap (i.e., ground subsidence). A concave up profile of soil arch between the vertical wall and the shear surface is then mobilized as illustrated in Fig. 2a, associated with the development of active lateral earth pressure. On the contrary, a retaining wall can be pushed into the retained soil. An inclined shear surface is mobilized, and a concave down profile of soil arch is formed, along with the occurrence of ground heave as shown in Fig. 2b. This is because the soil-wall interface is rough, which causes uneven soil deformations. From these illustration tests, one can see that the failure mechanism of soil wedge behind the wall is different from the assumption of Coulomb theory using a rigid failure wedge. This can partially explain why the Coulomb theory cannot calculate the lateral earth pressure accurately for retaining walls. It should be emphasized that the soil arch at different depth is different, and the mobilized soil shear strength should also vary with depth.

For pit-in-pit excavations, when the 2nd level retaining wall is close to the 1st level retaining wall, the mobilized soil arch will be confined between two parallel walls, and the full triangular-shaped failure wedge will become a trapezoidal-shaped failure wedge, as depicted in Fig. 3. Hu *et al.* [35] studied the behaviour of concave up shaped soil arch in the passive earth pressure zone between two parallel retaining walls (see Fig. 1) under the following assumptions: (a) the foundation soil is pure sand; (b) a concave up shaped major principal stress arch is formed when the wall moves to mobilize the full passive earth pressure; (c) the wall with a soil-wall interface friction angle of δ moves horizontally as a rigid body; (d) the inclined passive failure surface intersects the horizontal plane by an angle of $\beta = \pi/4 - \phi/2$ following the Rankine theory, where ϕ is soil friction angle; and (e) the 2nd level retaining wall has a high flexural rigidity, and its displacement is neglected.

The Rankine theory assumes that the wall is fully smooth. If the wall is rough, the inclination angle β will change. For a laterally moving wall, the plastic zone could develop to a depth below the base [30]. In this investigation (Fig. 3), the following assumptions are made to modify the analytical model of Hu *et al.* [35]: (a) the pit-in-pit excavation is simplified as a plane strain problem without considering the spatial effect; (b) clay can also be considered by converting

the cohesion into an equivalent friction angle; (c) the 2nd level retaining wall is simplified as a fixed boundary condition; (d) when the wall experiences a translational movement (T mode), the failure plane is assumed to initiate at a depth of $H/5$ from the base of the 2nd level retaining wall; (e) a rotational movement about its base (RB mode) can simplified as a T mode movement using the average wall displacement; (f) different size of major principal stress arch will be formed within the trapezoidal-shaped failure wedge.

The geometric model of a pit-in-pit excavation is presented in Fig. 3. The 1st level excavation reaches a depth of H_m from the ground surface, and the embedded depth of 1st level retaining wall after the 2nd level excavation is H. The failure plane OE initiates at a depth of $H' = H + H/5$ from the plane BC. The 2nd level retaining wall is within the trapezoidal-shaped failure wedge, and the depth BE above the wedge is H_1. The spacing between two parallel walls is defined as S. The 2nd level excavation will influence the passive earth pressure zone of the 1st level retaining wall when $(H' - H_1)\cot\beta \le S \le H'\cot\beta$. The inclination angle α of active earth pressure from the horizontal on the right side of the 1st level retaining wall can be calculated using the Coulomb theory, and the inclination angle β of passive failure surface OE on the left side of the 1st level retaining wall is now determined as:

$$\beta = \arctan\left\{\tan\phi \times \left[-1 + \sqrt{\cot\phi\cot(\phi+\delta)+1}\right]\right\} \quad (1)$$

where ϕ is the friction angle of soil, and δ represents the soil-wall interface friction angle.

B. FULL PASSIVE STATE

COHESIONLESS SOILS

The mechanism of soil arching between two retaining walls for pit-in-pit excavations is investigated as shown in Fig. 4a. The origin of the coordinate system is set at point C, and the y coordinate represents the depth of the passive earth pressure zone. A soil element AG with a thickness of dy and a width of S at a depth y is taken for analysis of the stress state. Based on the arching model of Handy [14], a horizontal soil element AG can be simulated as a major principal stress arch between two imaginary parallel walls as illustrated in Fig. 4b. Due to the boundary effect associated with the soil-wall interface friction, the major principal stress rotates (with a rotation angle θ from the horizontal at points A and G).

The Mohr circle at points A and G can then be drawn in Fig. 5. The line OG is tangent to the Mohr circle, which represents the shear strength envelope (with a friction angle of ϕ and a cohesion of $c = 0$ for cohesionless soils). The line OA rotates with an angle of δ from the horizontal. From Fig. 5a, one can derive the stress state at point A (i.e., σ_h is the horizontal stress, σ_v is the vertical stress, and τ_w is the shear stress,), when the maximum interface friction is mobilized as

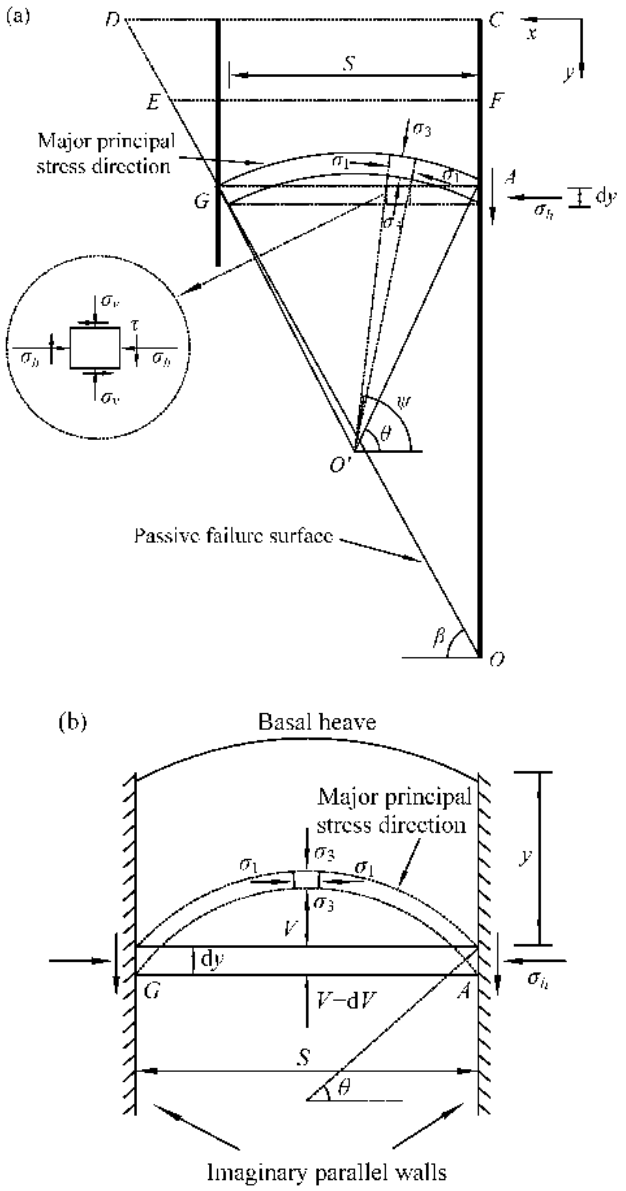

FIGURE 4. Mechanism of soil arching between two retaining walls for pit-in-pit braced excavations: (a) simplified passive earth pressure zone, and (b) major principal stress arch between two imaginary parallel walls.

follows:

$$\begin{cases} \sigma_h = \sigma_1 - \tau_w \cot\theta \\ \tau_w = (\sigma_1 - \sigma_3)\sin\theta cos\theta \\ \sigma_v = \sigma_1 \cos^2\theta + \sigma_3 \sin^2\theta \end{cases} \quad (2)$$

Eq. 2 can also be written as:

$$\begin{cases} \sigma_h = \sigma_3 \cos^2\theta + \sigma_1 \sin^2\theta \\ \sigma_v = \sigma_1 \cos^2\theta + \sigma_3 \sin^2\theta \end{cases} \quad (3)$$

By introducing the Rankine passive earth pressure coefficient $K_p = \sigma_1/\sigma_3 = \tan^2(\pi/4 + \phi/2)$, the lateral earth

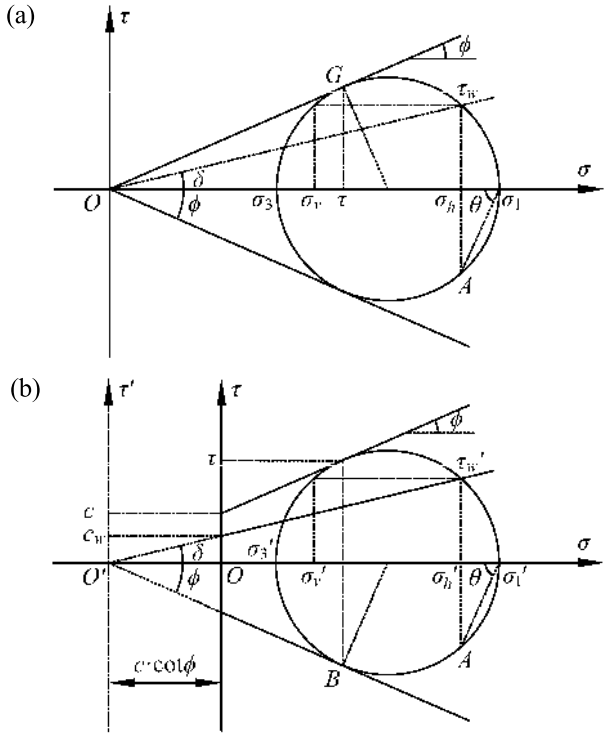

FIGURE 5. Mohr circle of major principal stress arch between imaginary parallel walls: (a) cohesionless soils, and (b) cohesive soils.

pressure coefficient at point A can be expressed by:

$$K = \frac{\sigma_h}{\sigma_v} = \frac{\cos^2\theta + K_p \sin^2\theta}{\sin^2\theta + K_p \cos^2\theta} \tag{4}$$

Following the similar procedure, the correlation between the horizontal stress σ_{mh} and the vertical stress σ_{mv} at an arbitrary point can be written as a function of the rotation angle of major principal stress from the horizontal ψ ($0 < \psi < \pi/2$).

$$\begin{cases} \sigma_{mh} = \sigma_3 \cos^2\psi + \sigma_1 \sin^2\psi \\ \sigma_{mv} = \sigma_1 \cos^2\psi + \sigma_3 \sin^2\psi \end{cases} \tag{5}$$

From Fig. 4b, one can see that the vertical stress on a horizontal soil element is not uniformly distributed. Hence, the average vertical stress $\sigma_{av} = V/S$ is calculated for use to derive the passive earth pressure coefficient $K_{wp} = \sigma_h/\sigma_{av}$. The term σ_{av} can be estimated by an integration over the whole arch using in polar coordinates. As shown in Fig. 4a, the radius of the arch R can be expressed by $R = S/2cos\theta$. The vertical force acting on an element of the arch is then calculated by $\mathrm{d}V = \sigma_{mv}\mathrm{d}s = \sigma_{mv}R\sin\psi\mathrm{d}\psi$. Hence, the term σ_{av} is computed by:

$$\begin{aligned} \sigma_{av} &= \frac{1}{S}\int_0^S dV = \frac{2}{S}\int_\theta^{\frac{\pi}{2}} \sigma_{mv} R sin\psi d\psi \\ &= \frac{1}{6}\left[2\sigma_1 \cos^2\theta - \sigma_3(\cos 2\theta - 5)\right] \end{aligned} \tag{6}$$

The passive earth pressure coefficient is now written as:

$$K_{wp} = \frac{\sigma_h}{\sigma_v} = \frac{3\left(\cos^2\theta + K_p \sin^2\theta\right)}{\left(3 - \cos^2\theta\right) + K_p \cos^2\theta} \tag{7}$$

where the rotation angle θ of major principal stress can be calculated from the geometric relationship as presented in Fig. 5a by:

$$\theta = \arctan \frac{K_p - 1 + \sqrt{\left(K_p - 1\right)^2 - 4K_p \tan^2\delta}}{2K_p \tan\delta} \tag{8}$$

It can be seen from Eq. 7 that the spacing between two parallel walls has no influence on the calculation of K_{wp} for cohesionless soils.

COHESIVE SOILS

For cohesive soils, the shear strength parameter of cohesion c needs to be incorporated into the derivation of passive earth pressure coefficient. Due to the soil-wall interface friction, the apparent cohesion c_w is then derived by:

$$c_w = c\tan\delta/\tan\phi \tag{9}$$

Equivalent shear strength parameters (i.e., equivalent friction angle ϕ_d) are often defined for cohesive soils, such that cohesive soils will have equivalent properties of cohesionless soils. For example, Ni *et al.* [27] suggested to derive the equivalent friction angle based on the assumption of equal shear strength as follows:

$$\phi_d = \arctan\left(\tan\phi + \frac{c}{\gamma h}\right) \tag{10}$$

where γ is the unit weight of the soil, and h denotes the depth. This expression is simply, but the calculated ϕ_d value becomes unrealistic especially for shallow depth.

Similarly, Ni *et al.* [27] calculated the ϕ_d value by assuming that the Rankine earth pressure is equal:

$$\phi_d = 2\left(\arctan\left[\tan\left(\frac{\pi}{4} + \frac{\phi}{2}\right) - \frac{2c}{\gamma h}\right] - \frac{\pi}{4}\right) \tag{11}$$

However, the assumption of equal earth pressure will become invalid for the calculation of earth pressures considering soil arching.

In this investigation, coordinate transforms are used to compute the ϕ_d value for cohesive soils based on the shear strength envelope. As presented in Fig. 5b, the cohesion intercept of c_w in the coordinate system with an origin at point O (i.e., normal stress σ and shear stress τ) will become zero in the shifted coordinate system with an origin at point O' (i.e., normal stress σ' and shear stress τ'). The shift of the coordinate can be calculated as an additional term of normal stress of $c\cdot\cot\phi$. Therefore, the stress state at an arbitrary point can now be written as:

$$\begin{cases} \sigma = \sigma' - c\cdot\cot\phi \\ \tau = \tau' \end{cases} \tag{12}$$

TABLE 1. Approximate displacement required to mobilize the full passive earth pressure.

Type of Backfill	Clough and Duncan [36]	Becker and Moore [37]
Dense sand	$0.01{\cdot}H$	$0.02{\cdot}H$
Medium sand	$0.02{\cdot}H$	–
Loose sand	$0.04{\cdot}H$	$0.06{\cdot}H$
Stiff cohesive	–	$0.02{\cdot}H$
Soft cohesive	–	$0.04{\cdot}H$
Compacted silt	$0.02{\cdot}H$	–
Compacted lean clay	$0.05{\cdot}H$	–
Compacted fat clay	$0.05{\cdot}H$	–

H: height of wall

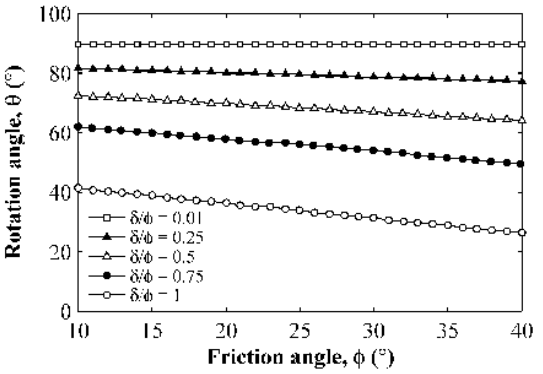

FIGURE 6. Influence of interface roughness on the rotation angle of major principal stress.

Following the same procedure for cohesionless soils, the passive earth pressure coefficient K'_{wp} for cohesive soils is now expressed by:

$$K'_{wp} = \frac{\sigma_h}{\sigma_{av}} = \frac{\sigma'_h - c\cot\phi}{\sigma'_{av} - c\cot\phi} = \frac{3\left(\cos^2\theta + K_p\sin^2\theta\right) - \frac{3c}{\gamma y\tan\phi + c}}{3 - cos^2\theta + K_p\cos^2\theta - \frac{3c}{\gamma y\tan\phi + c}} \tag{13}$$

For a perfectly smooth wall (i.e., $\delta = 0$), Eq. 13 reduces to the Rankine coefficient by:

$$K'_{wp} = \tan^2\left(\frac{\pi}{4} + \frac{\phi}{2}\right) + \frac{2c}{\gamma y}\tan\left(\frac{\pi}{4} + \frac{\phi}{2}\right) \tag{14}$$

C. INTERMEDIATE PASSIVE STATE

The mobilized passive earth pressure is a function of wall movement [25]. In practice, the full passive state cannot always be mobilized, and the soil between two retaining walls for pit-in-pit excavations can be at the intermediate passive state (the state between passive and at-rest). Table 1 summarizes the approximate wall movement required to mobilize the full passive earth pressure (s_p) for different types of soils. The actual wall movement can be specified a fraction of the full displacement ($\eta \cdot s_p$, where $\eta \in [0, 1]$). When the η value changes from 0 to 1, the friction angles of soil and the soil-wall interface develop from ϕ_0 and δ_0 at the initial passive state to ϕ and δ at the full passive state. Along with the wall movement, the failure surface initiates and propagates. The parameters of ϕ_m and δ_m at any intermediate passive state can be written as:

$$\begin{cases} \tan\phi_m = \tan\phi_0 + \dfrac{4}{\pi}\arctan\eta \times (\tan\phi - \tan\phi_0) \\ \tan\delta_m = \tan\delta_0 + \dfrac{4}{\pi}\arctan\eta \times (\tan\delta - \tan\delta_0) \end{cases} \tag{15}$$

The mobilized cohesion c_m can be calculated from the apparent cohesion c_w as follows:

$$c_m = \frac{\tan\phi_m}{\tan\phi}c_w \tag{16}$$

The parameters of ϕ_0 and δ_0 at the initial passive state can be estimated based on the Coulomb theory by:

$$\frac{1}{K_0} = \frac{1}{1-\sin\phi} = \left(\frac{1}{\cos\phi_0} + \sqrt{\tan^2\phi_0 + \tan\phi_0\tan\delta_0}\right)^2 \tag{17}$$

where K_0 is the lateral earth pressure coefficient at-rest. The initial interface friction angle δ_0 can be conservatively estimated by $\phi_0/2$ [38].

Therefore, the passive earth pressure coefficient at any intermediate state K_{wpm} can be derived by replacing ϕ, δ and c at the full passive state with ϕ_m, δ_m, and c_m in Eq. 7 for cohesionless soils as follows:

$$K_{wpm} = \frac{3\left(\cos^2\theta_m + K_{pm}\sin^2\theta_m\right)}{\left(3 - \cos^2\theta_m\right) + K_{pm}\cos^2\theta_m} \tag{18}$$

Similarly, Eq. 13 can be extended for cohesive soils at any intermediate passive state by:

$$K'_{wpm} = \frac{3\left(\cos^2\theta_m + K_{pm}\sin^2\theta_m\right) - \frac{3c_m}{\gamma y\tan\phi_m + c_m}}{3 - cos^2\theta_m + K_{pm}\cos^2\theta_m - \frac{3c_m}{\gamma y\tan\phi_m + c_m}} \tag{19}$$

where the rotation angle of major principal stress θ_m and the Rankine lateral earth pressure coefficient K_{pm} are calculated by:

$$\begin{cases} \theta_m = \arctan\dfrac{K_{pm} - 1 + \sqrt{\left(K_{pm}-1\right)^2 - 4K_{pm}\tan^2\delta_m}}{2K_{pm}\tan\delta_m} \\ K_{pm} = \tan^2\left(\dfrac{\pi}{4} + \frac{\phi_m}{2}\right) \end{cases} \tag{20}$$

D. COMPARISON AGAINST COULOMB AND RANKINE THEORIES

The correlation between rotation angle of major principal stress θ and soil friction angle ϕ is calculated in Fig. 6 for different degree of roughness at the soil-wall interface (δ/ϕ). It can be seen that when the soil-wall interface is perfectly smooth ($\delta/\phi = 0.01$), the θ value is 90°, and the direction of

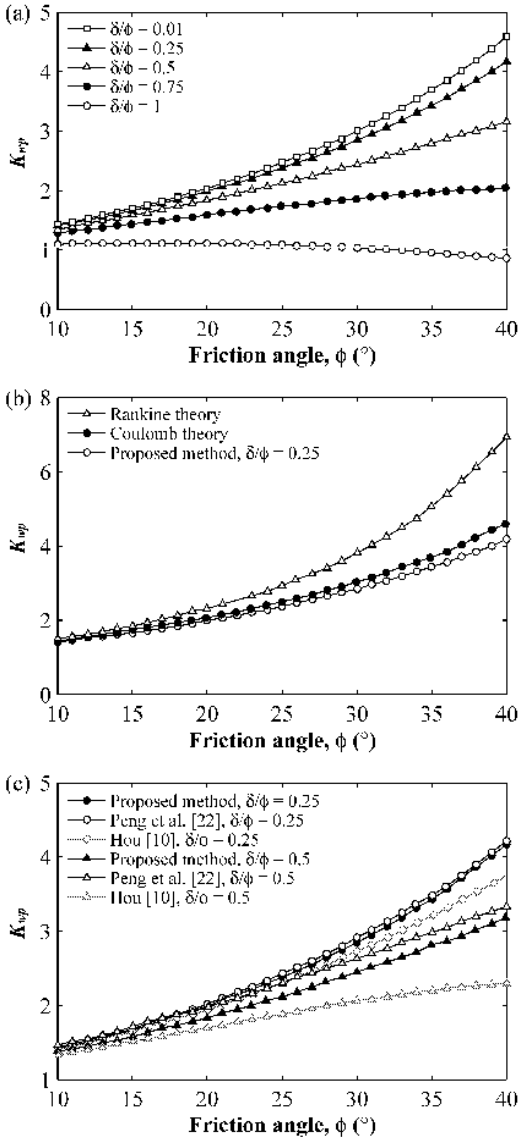

FIGURE 7. Passive earth pressure coefficient: (a) influence of interface roughness, (b) comparison against classical Coulomb and Rankine theories, and (c) comparison against other analytical solutions.

major principal stress is parallel to the vertical wall. The stress state of the major principal stress arch follows the Rankine theory, where θ is independent of ϕ. With the increase of interface roughness, the θ value decreases, and the major principal stress deviates from the vertical plane more ($90°$–θ). For higher values of δ and ϕ, the major principal stress rotates more, and the soil arching effect becomes more dominant.

In Fig. 7, the variations of earth pressure coefficient K_{wp} at the full passive state for cohesionless soils with soil friction angle are evaluated. It is interesting to notice in Fig. 7a that the K_{wp} value decreases with ϕ for a perfectly rough wall ($\delta/\phi = 1$). This is probably induced by the confining effect of rough wall on the rotation angle of major principal stress, where a significant rotation causes stress relaxation within the soil. When the wall becomes smoother (δ/ϕ decreases),

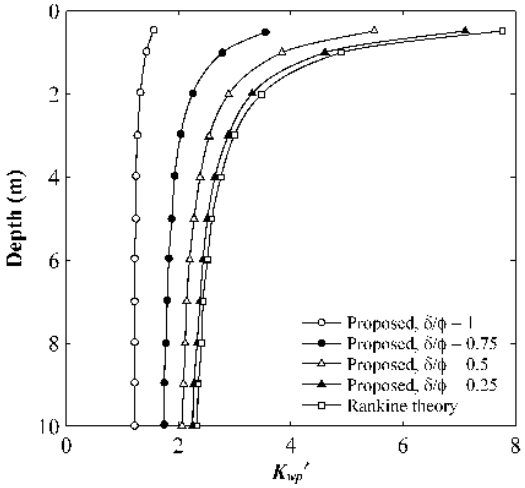

FIGURE 8. Variation of passive earth pressure coefficient with depth of retaining wall.

tbe K_{wp} value becomes an increasing function of ϕ. For $\delta/\phi = 0.25$, the calculated pattern of the K_{wp} using the proposed solution is compared with those estimated using the Coulomb and Rankine theories in Fig. 7b. The calculated curve shows a trend similar, which is closer to the Rankine theory. This is anticipated since the soil arching effect is not considered in the Coulomb theory. In Fig. 7c, the efficacy of the proposed approach is compared against calculations using the methods of Peng *et al.* [23] and Hou [15]. Peng *et al.* [23] assumed a parabolic major principal stress arch and incorporated the θ value in their calculation. Hou [15] simply modified the Handy arching model using depth-dependent vertical stress above a horizontal soil element. The proposed solution agrees well with the method of Peng *et al.* [23], but is higher than the method of Hou [15].

For cohesive soils, the calculation of earth pressure coefficient K'_{wp} at the full passive state is dependent on soil shear strength parameters ($c = 20$ kPa and $\phi = 20°$), unit weight ($\gamma = 20$ kN/m^3), wall roughness ($\delta/\phi = 0.5$), and depth ($H = 10$ m). Fig. 8 plots the pattern of K'_{wp} as a function of wall roughness and depth. It is clear that the proposed method deviates from the Rankine theory significantly at shallow depth, but the difference decreases with depth. It should be emphasized that the K'_{wp} value at shallow depth is unrealistic for both the proposed method and the Rankine theory. For a smaller confining pressure at shallow depth, the magnitude of cohesion should be negligible. However, cohesion is often computed by the intercept of the shear strength envelope from Mohr circle, and this process will cause an unrealistic determination of cohesion at shallow depth. Again, the proposed solution approaches the Rankine theory for a perfectly smooth wall.

The proposed solution is capable of evaluating the earth pressure coefficient K_{wpm} at any intermediate passive state. Fig. 9 shows the mobilized shear strength parameters as a function of displacement ratio η of retaining wall. With the increase of η, both the friction angle ratio ϕ_m/ϕ and the

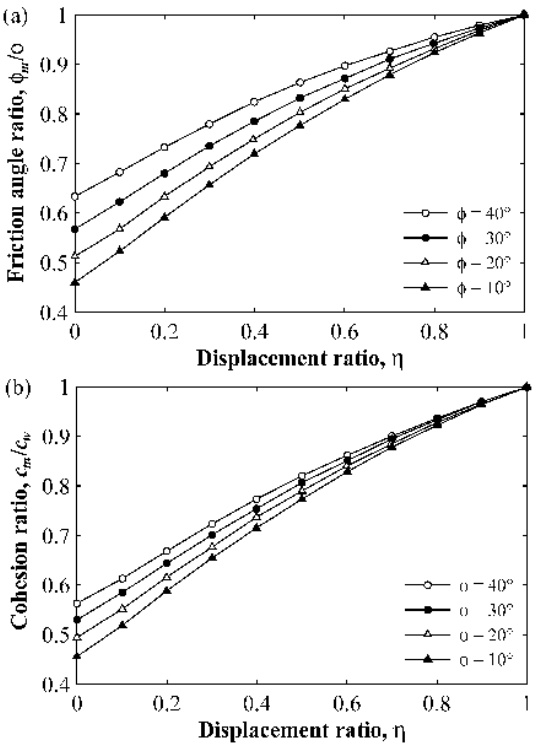

FIGURE 9. Correlation of soil shear strength parameters and displacement ratio of retaining wall: (a) mobilized friction angle ratio, and (b) mobilized cohesion ratio.

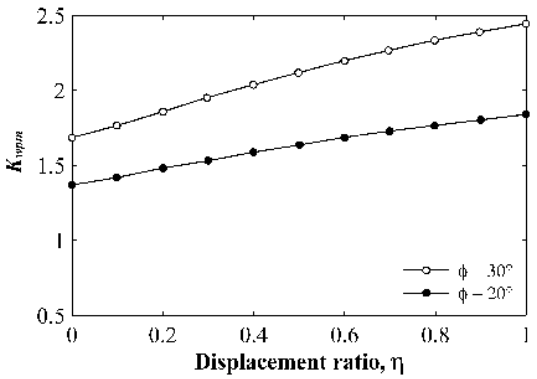

FIGURE 10. Variation of passive earth pressure coefficient with displacement ratio of retaining wall.

cohesion ratio c_m/c increase. The values of ϕ_m/ϕ and c_m/c eventually approach 1 for $\eta = 1$. Fig. 10 illustrates the relation between K_{wpm} and η for cohesionless soils with a friction angle of $\phi = 20°$ and $\phi = 30°$. The K_{wpm} value at any intermediate passive state increases nonlinearly with the increase of η. For $\eta = 0$, the K_{wpm} value reduces to the lateral earth pressure at-rest K_0; whereas for $\eta = 1$, the earth pressure coefficient K_{wp} at the full passive state is mobilized.

III. PASSIVE EARTH PRESSURE CONSIDERING SOIL ARCHING

With the theoretical bases by Section II, this section derives the closed-form solutions for passive earth pressures at intermediate and full states considering soil arching effects. The developed model is then explored by carrying out a parametric study.

A. COHESIONLESS SOILS AT THE FULL PASSIVE STATE

The trapezoidal-shaped failure wedge *OCBE* in Fig. 3 is taken out and plotted in Fig. 11a, and all geometric parameters preserve the same definitions. The failure wedge can be divided into a rectangular zone above the base *EF* of the 2nd level retaining wall and a triangular zone below the base *EF*. Hu *et al.* [35] assumed that a complete symmetric arch will be formed in the rectangular zone with the base of the arch acting on two parallel walls, and a half arch will be formed in the rectangular zone with the top of the arch passing through the inclined shear surface. For the soil arch in the rectangular area, a half arch will be formed in the stable zone outside the failure wedge. In this investigation, the shape of soil arch in the rectangular area is modified as given in Fig. 3, where one base acts on the 1st level retaining wall and another base acts on the inclined shear surface. To distinguish between solutions, the subscripts 1 and 2 are defined to denote the calculated stresses in the rectangular and triangular zones, respectively.

As shown in Fig. 11b, a soil element with a thickness of dy at a depth y in the rectangular zone *BCFE* is analyzed. The width B of the soil element can be calculated as:

$$B = S \quad \text{for } y < H_1 \tag{21}$$

The soil element is subjected to confinement and friction at the soil-wall interface. Due to the rotation of major principal stress, the soil arching effect will induce ground heave, resulting in a difference of vertical stress acting above and below the soil element. The force equilibrium in the vertical direction is then established:

$$\begin{aligned} Bd\sigma_{av1} - 2\mu\sigma_{h1}dy &= dW \\ &= Bd\sigma_{av1} - 2\mu K_{wp}\sigma_{av1}dy \\ &= \gamma B dy \end{aligned} \tag{22}$$

where σ_{av1} is the average vertical stress acting above the soil element, μ denotes the interface friction coefficient ($\mu = \tan\delta$), σ_{h1} is the horizontal stress due to the confinement of the wall, dW represents the self-weight of the soil element (d$W = \gamma B$dy), and K_{wp} is the earth pressure coefficient at the full passive state.

The governing differential equation for σ_{av1} with respect to depth y is then derived:

$$\frac{d\sigma_{av1}}{dy} = \frac{2\mu K_{wp}\sigma_{av1}}{B} + \gamma \tag{23}$$

By substituting the boundary condition of $\sigma_{av1} = 0$ at $y = 0$, the solution of average vertical stress σ_{av1} can be derived by integrating Eq. 23. The average horizontal stress σ_{h1} is also derived.

$$\sigma_{av1} = \frac{\gamma S}{2\mu K_{wp}}\left[\exp\left(\frac{2\mu K_{wp}y}{S}\right) - 1\right] \tag{24}$$

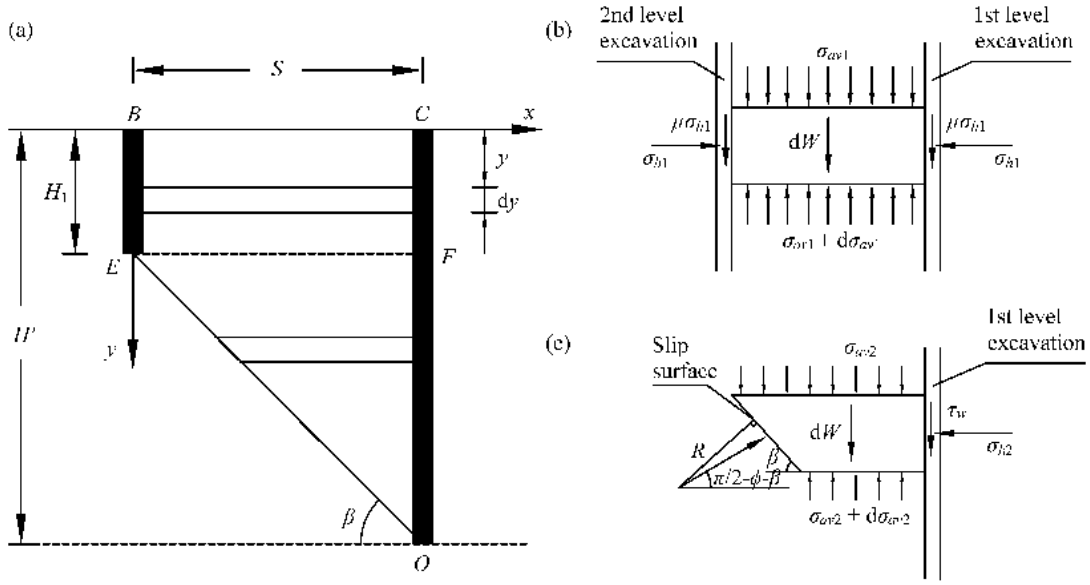

FIGURE 11. Model for calculating earth pressure for pit-in-pit excavations: (a) trapezoidal-shaped failure wedge, (b) soil element in the rectangular zone *BCFE*, and (c) soil element in the triangular zone *OEF*.

$$\sigma_{h1} = \sigma_{av1} K_{wp} = \frac{\gamma S}{2\mu}\left[\exp\left(\frac{2\mu K_{wp} y}{S}\right) - 1\right] \quad (25)$$

Similarly, a soil element in the triangular zone OEF is plotted in Fig. 11c. The resultant force acting on the failure surface is denoted by R. The average vertical and horizontal stresses are expressed by σ_{av2} and σ_{h2}. The mobilized shear stress at the soil-wall interface is defined by $\tau_w = \sigma_{h2} \tan\delta$. The width B of the soil element is now expressed by:

$$B = \left(H' - y\right)\cot\beta \quad \text{for } (y \geq H_1) \quad (26)$$

The horizontal and vertical force equilibrium conditions are now written as:

$$\sigma_{h2} dy - R\cos\left(\frac{\pi}{2} - \beta - \phi\right) dy = 0 \quad (27)$$

$$dW + \tau_w dy - R\sin\left(\frac{\pi}{2} - \beta - \phi\right) dy - d\left[\sigma_{av2}\left(H' - y\right)\right]\cot\beta = 0 \quad (28)$$

where the self-weight of the soil element is calculated by

$$dW = \frac{\gamma}{2}\left[\left(H' - y\right)\cot\beta + \left(H' - y - dy\right)\cot\beta\right] dy \quad (29)$$

Combining Eqs. 27-29, the differential equation for σ_{av2} with respect to y is obtained:

$$\frac{d\sigma_{av2}}{dy} = \frac{\sigma_{av2}}{H' - y}\left[1 + \frac{\tan\delta - \cot(\beta + \phi)}{\cot\beta} K_{wp}\right] + \gamma = \frac{A\sigma_{av2}}{H' - y} + \gamma \quad (30)$$

in which, the parameter A is defined as

$$A = 1 + \frac{\tan\delta - \cot(\beta + \phi)}{\cot\beta} K_{wp} \quad (31)$$

The stress state at the interface between the rectangular and the triangular zones should be continuous. Therefore, the boundary condition is $\sigma_{av2}|_{y=H_1} = \sigma_{av1}|_{y=H_1} = q$.

$$q = \frac{\gamma S}{2\mu K_{wp}}\left[\exp\left(\frac{2\mu K_{wp} H_1}{S}\right) - 1\right] \quad (32)$$

The average vertical stress σ_{av2} and the average horizontal stress σ_{h2} are now derived as:

$$\sigma_{av2} = \frac{\left(H' - H_1\right)^A \left(q + Aq + H'\gamma - H_1\gamma\right) - \left(H' - vy\right)^{A+1}\gamma}{(A+1) \times (H' - y)^A} \quad (33)$$

$$\sigma_{h2} = \sigma_{av2} K_{wp} = \frac{(H' - H_1)^A (q + Aq + H'\gamma - H_1\gamma) - (H' - y)^{A+1}\gamma}{(A+1) \times (H' - y)^A} K_{wp} \quad (34)$$

B. COHESIVE SOILS AT THE FULL PASSIVE STATE

For cohesive soils, the earth pressure coefficient K'_{wp} at the full passive state is a function of depth y, and the calculation of earth pressures using Eq. 13 will be very complicated. A term of $\sigma_0 = c/tan\phi$ is proposed to characterize the strength due to cohesion. The mobilized shear stress should be revised by incorporating the effect of cohesion.

$$\tau_w = (\sigma_h + \sigma_0)\tan\delta = \sigma'_h \tan\delta = K_{wp}\sigma'_{av}\tan\delta = K_{wp}(\sigma_{av} + \sigma_0)\tan\delta \quad (35)$$

Hereafter, the depth-dependent K'_{wp} is replaced by the passive earth pressure coefficient K_{wp} for cohesionless soils as reported in Eq. 7. Following the same procedure, the differential equation for σ_{av1} with respect to depth y in the rectangular

zone is written as:

$$\frac{d\sigma_{av1}}{dy} = \frac{2\left(a\sigma_{av1}+b\right)}{S} + \gamma \tag{36}$$

where the parameters a and b are defined by $a = K_{wp}\tan\delta$ and $b = \sigma_0 K_{wp}\tan\delta = a\sigma_0$.

Using the boundary condition of $\sigma_{av1}|_{y=0} = 0$, the average vertical and horizontal stresses are calculated as follows:

$$\sigma_{av1} = \frac{\left(e^{2ay/S}-1\right)\left(2b+S\gamma\right)}{2a} \tag{37}$$

$$\sigma_{h1} = \sigma_{av1}K'_{wp} = \frac{\left(e^{2ay/S}-1\right)\left(2b+S\gamma\right)}{2a}K'_{wp} \tag{38}$$

In the triangular zone, the differential equation of σ_{av2} with respect to depth y has the following form:

$$\begin{aligned}\frac{d\sigma_{av2}}{dy} = {} & \frac{\sigma_{av2}}{H'-y}\left[\frac{\tan\delta-\cot\left(\beta+\phi\right)}{\cot\beta}K_{wp}+1\right] \\ & + \frac{\sigma_0}{H'-y}\left[\frac{\tan\delta-\cot\left(\beta+\phi\right)}{\cot\beta}K_{wp}\right. \\ & \left. + \frac{\cot\left(\beta+\phi\right)}{\cot\beta}\right] + \gamma\end{aligned} \tag{39}$$

Three parameters of A, σ_0 and D are defined to simply the calculation.

$$\begin{cases} A = \dfrac{\tan\delta-\cot\left(\beta+\phi\right)}{\cot\beta}K_{wp}+1 \\ \sigma_0 = c\cot\phi \\ D = \left[\dfrac{\tan\delta-\cot\left(\beta+\phi\right)}{\cot\beta}K_{wp}+\dfrac{\cot\left(\beta+\phi\right)}{\cot\beta}\right]\sigma_0 \end{cases} \tag{40}$$

Due to the stress compatibility at the depth H_1 $\left(\sigma_{av2}|_{y=H_1} = \sigma_{av1}|_{y=H_1} = q\right)$, the average vertical and horizontal stresses are determined by:

$$\begin{aligned}\sigma_{av2} = {} & \frac{\left(H'-H_1\right)^A\left[\left(1+A\right)\left(D+Aq\right)+A\left(H'-H_1\right)\gamma\right]}{A\left(1+A\right)\left(H'-y\right)^A} \\ & - \frac{\left(H'-y\right)^A\left[\left(1+A\right)D+A\left(H'-y\right)\gamma\right]}{A\left(1+A\right)\left(H'-y\right)^A}\end{aligned} \tag{41}$$

$$q = \frac{\left(e^{2aH_1/S}-1\right)\left(2b+S\gamma\right)}{2a} \tag{42}$$

$$\sigma_{h2} = \sigma_{av2}K'_{wp} \tag{43}$$

C. INTERMEDIATE PASSIVE EARTH PRESSURE

At any intermediate passive state, the mobilized shear strength parameters of soil are dependent on the displacement ratio of retaining wall, but do not change with the depth. Hence, the parameters ϕ_m, c_m, δ_m, and K_{wpm} and K'_{wpm} are used to replace the corresponding values in the derivations of passive earth pressures at the full passive state. The results are summarized as follows:

- Cohesionless soils:

$$\sigma_{h1} = \frac{\gamma S}{2\mu}\left[\exp\left(\frac{2\mu K_{wpm}y}{S}\right)-1\right] \tag{44}$$

$$\begin{aligned}\sigma_{h2} = {} & \frac{\left(H'-H_1\right)^A\left(q+Aq+H'\gamma-H_1\gamma\right)-\left(H'-y\right)^{A+1}\gamma}{\left(A+1\right)\times\left(H'-y\right)^A} \\ & \times K_{wpm}\end{aligned} \tag{45}$$

$$A = 1+\frac{\tan\delta_m-\cot\left(\beta+\phi_m\right)}{\cot\beta}K_{wpm} \tag{46}$$

$$q = \frac{\gamma S}{2\mu K_{wpm}}\left[\exp\left(\frac{2\mu K_{wpm}H_1}{S}\right)-1\right] \tag{47}$$

- Cohesive soils:

$$\sigma_{h1} = \frac{\left(e^{2ay/S}-1\right)\left(2b+S\gamma\right)}{2a}K'_{wpm} \tag{48}$$

$$\begin{aligned}\sigma_{h2} = {} & \frac{\left(H'-H_1\right)^A\left[\left(1+A\right)\left(D+Aq\right)+A\left(H'-H_1\right)\gamma\right]}{A\left(1+A\right)\left(H'-y\right)^A} \\ & \times K'_{wpm} \\ & - \frac{\left(H'-y\right)^A\left[\left(1+A\right)D+A\left(H'-y\right)\gamma\right]}{A\left(1+A\right)\left(H'-y\right)^A}K'_{wpm}\end{aligned} \tag{49}$$

$$\begin{cases} A = \dfrac{\tan\delta_m-\cot\left(\beta+\phi_m\right)}{\cot\beta}K_{wpm}+1 \\ \sigma_0 = c\cot\phi_m \\ D = \left[\dfrac{\tan\delta_m-\cot(\beta+\phi_m)}{\cot\beta}K_{wpm}+\dfrac{\cot(\beta+\phi_m)}{\cot\beta}\right]\sigma_0 \\ a = K_{wpm}\tan\delta_m \end{cases} \tag{50}$$

$$q = \frac{\left(e^{2aH_1/S}-1\right)\left(2b+S\gamma\right)}{2a} \tag{51}$$

D. PARAMETRIC STUDY

In the following, a case of pit-in-pit excavation is analyzed using the proposed approach. The 1st level retaining wall has an embedded depth of $H = 12$ m, and the spacing between two parallel walls is $S = 12$ m. The backfill is pure sand, with a unit weight of $\gamma = 18.5$ kN/m^3, and a friction angle of $\phi = 28°$. The wall roughness is defined by an interface friction angle of $\delta = \phi/2 = 14°$. For comparison, the calculation for cohesive soil by introducing a cohesion of $c = 10$ kPa is also conducted, whereas other parameters are kept constant.

Fig. 12 shows the comparison of depth-dependent passive earth pressures at the full passive state calculated using different approaches. It should be noted that the triangular zone is determined to initiate at a depth $H_1 = 7.2$ m. The calculated curve using the proposed method shows a linear pattern at shallow depth above H_1; whereas a highly nonlinear pattern is observed below H_1. The calculated value generally falls between the two extreme limits defined by the Coulomb and Rankine theories. At greater depth, the current solution estimates the earth pressure that is smaller than that computed using the method of Hu *et al.* [35]. The difference could be induced by different definition of soil arch in the triangular zone. At any intermediate state, the variations of passive earth pressure with depth are calculated as given in Fig. 13. It can be seen that a greater passive earth pressure is mobilized when the displacement of the wall increases (η increases). Frictions between the foundation soil and the wall increase with η,

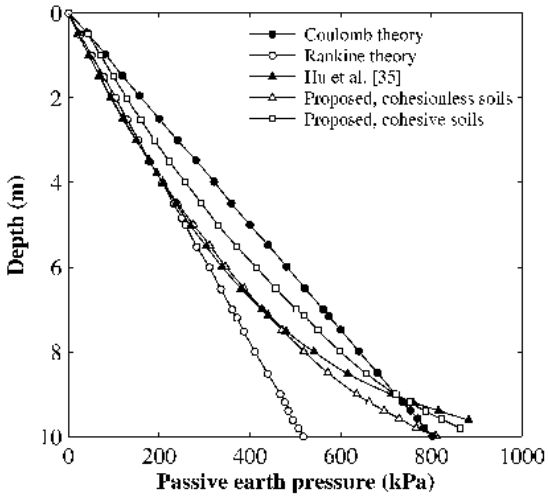

FIGURE 12. Comparison of passive earth pressure with depth of retaining wall calculated using different methods.

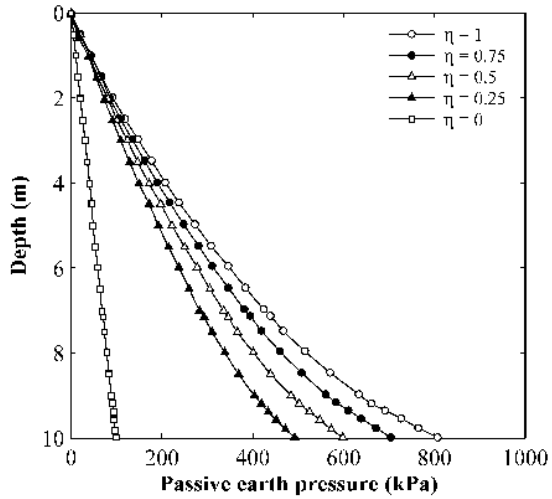

FIGURE 13. Variation of passive earth pressure with displacement ratio for cohesionless soils.

resulting in more significant soil arching effect. Therefore, the distribution of passive earth pressure becomes highly nonlinear. By integration over the depth, the percentage of resultant thrust and overturning moment acting on the wall at any intermediate passive state over those at the full passive state is calculated in Fig. 14. As expected, the response of the wall is gradually mobilized with the increase of wall movement. The thrust and overturning moment can be scaled up a factor of 5 from the at-rest state to the full passive state.

The influence of soil shear strength parameters on the mobilized earth pressure acting on the wall at the intermediate passive state is investigated in Fig. 15 for three types of cohesive soils. All soil parameters are tabulated in Table 2. It demonstrates that when the foundation soil has a higher shear strength (higher friction angle and cohesion), a higher passive resistance (earth pressure) is calculated. Therefore, when the foundation soil does not have adequate

TABLE 2. Three types of cohesive soils.

Type	γ (kN/m^3)	c (kPa)	ϕ (°)	δ/ϕ
Soil 1	16.5	5.0	10.0	0.75
Soil 2	17.8	12.2	13.4	0.75
Soil 3	18.7	16.5	17.9	0.75
Soil 4	19.8	20.7	22.5	0.75
Soil 5	20.5	40.0	40.0	0.75

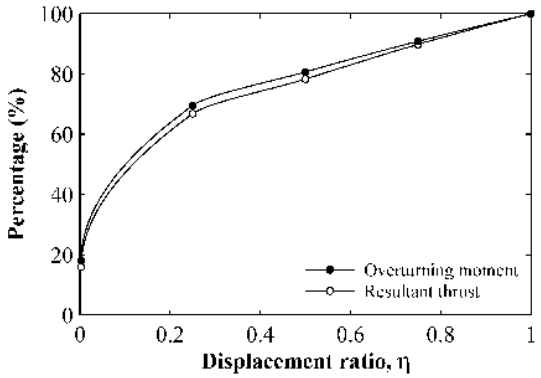

FIGURE 14. Percentage of resultant thrust and overturning moment acting on the retaining wall at any intermediate passive state over those at the full passive state.

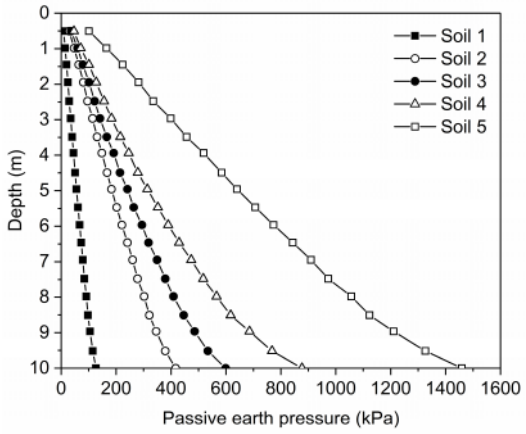

FIGURE 15. Influence of soil shear strength on the development of passive earth pressure acting on the retaining wall.

shear strength, treatment should be implemented to minimize the adverse impact of 2nd level excavation on the stability of 1st level retaining wall for pit-in-pit excavations.

The influence range of soil arching effect can be evaluated by $H' \cdot \cot\beta$. If the spacing S between two parallel walls is less than $H' \cdot \cot\beta$, the proposed method is applicable for calculating passive earth pressures on the wall for pit-in-pit excavations. Otherwise, introducing a 2nd level retaining wall at a distance of $S > H' \cdot \cot\beta$ will not influence the stability of 1st level retaining wall. Fig. 16 draws a diagram for use in design to evaluate the magnitude of $H' \cdot \cot\beta$. As expected,

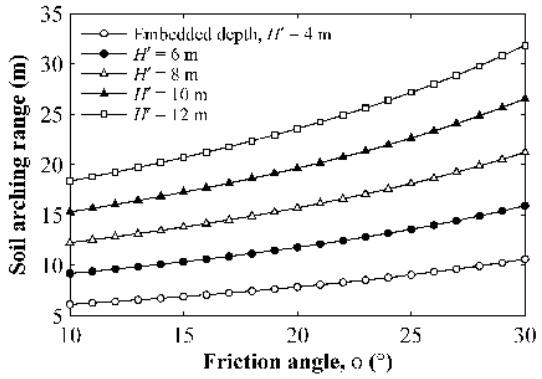

FIGURE 16. Variation of soil arching range with embedded depth of 1st level retaining wall and soil friction angle.

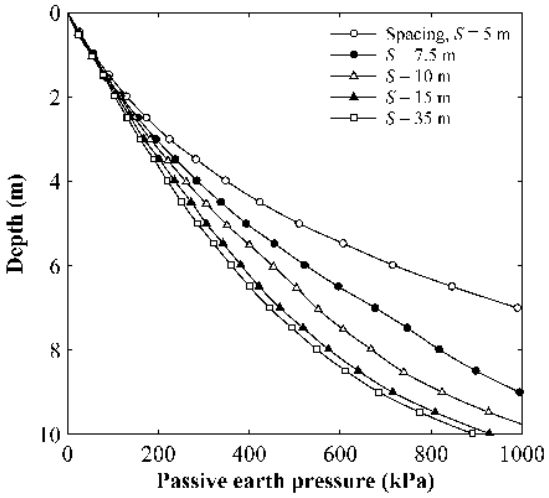

FIGURE 17. Correlation of passive earth pressure acting on the retaining wall and the spacing between two retaining walls.

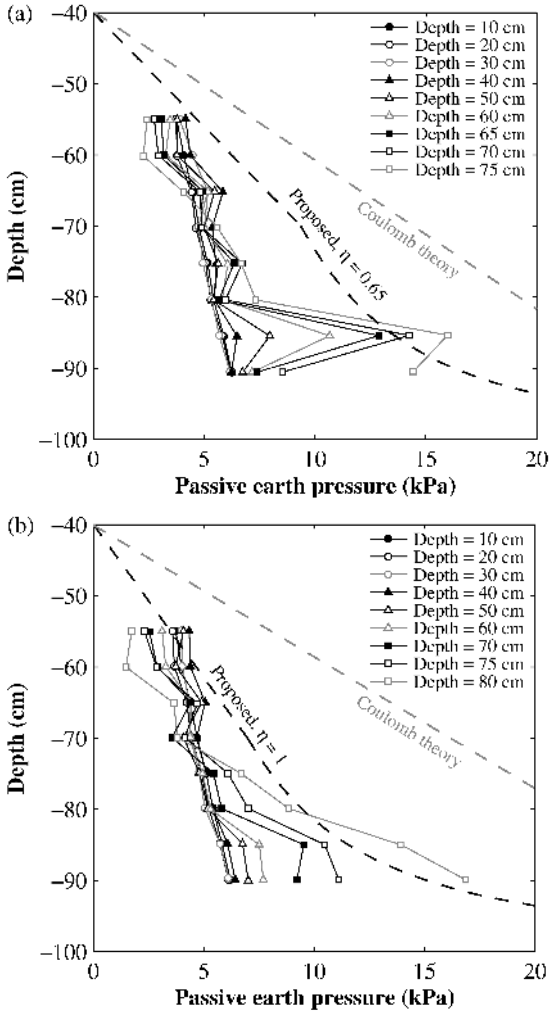

FIGURE 18. Measured versus calculated passive earth pressure for pit-in-pit excavations: (a) model test MG1, and (b) model test MG2. (Experiment data are taken from Zheng *et al.* [10]).

for a greater embedded depth H' or a higher friction angle, the allowable spacing between two walls is increased.

The correlation of passive earth pressure acing on the wall and the spacing between two walls is plotted in Fig. 17. From Fig. 16, the allowable spacing can be interpreted as $H' \cdot \cot\beta = 24.8$ m for the 1st level retaining wall with an embedded depth of $H' = 10$ m buried in the soil with a friction angle of $\phi = 28°$. It can be seen that when the spacing S is less than 24.8 m, the pattern of passive earth pressure shifts to the left, where the mobilized earth pressure becomes smaller at a specific depth with the increase of spacing. At a large spacing, the results of earth pressure become converge. For pit-in-pit excavations, when the spacing between two walls is small, horizontal struts should be designed to resist the mobilized passive earth pressure.

IV. COMPARISON AGAINST EXPERIMENTAL MEASUREMENTS

Zheng *et al.* [10] performed a series of model-scale tests for pit-in-pit excavations, where retaining piles were heavily instrumented with earth pressure cells and buried in a test apparatus with dimensions of 2.5 m × 2.46 m × 1.4 m (length × width × height). The backfill soil was pure sand with particle size smaller than 2 mm. Two tests with geometric and soil shear strength parameters as listed in Table 3 are analyzed in this study to demonstrate the effectiveness of the proposed analytical solution. Fig. 18 illustrates the comparison of measured and calculated passive earth pressures. It should be noted that the excavation was implemented in steps during the tests. The measured earth pressures in Fig. 18 represent the values obtained for different piles at all steps. The purpose of the comparison is to check whether the proposed approach can reproduce the maximum profile of passive earth pressure. Therefore, experimental measurements in different steps are not distinguished. Calculations based on the conventional Coulomb theory are also conducted. It can be seen that the Coulomb theory always overestimates the passive earth pressure, whereas the proposed technique can produce results that are much closer to experimental data. This is because

TABLE 3. Geometric and soil shear strength parameters for the model tests of Zheng *et al.* [10].

Test	H' (cm)	H_1 (cm)	S (cm)	γ (kN/m^3)	c (kPa)	ϕ (°)	δ/ϕ
MG1	60	30	10	15.5	0	31	0.9
MG2	60	30	20	15.5	0	35.6	1

the 2nd level retaining wall does intersect the inclined failure plane, and the proposed method can take into account the soil arching effect properly.

V. CONCLUSIONS

Pit-in-pit excavations become more and more popular due to the demand for underground space utilization especially for urban areas in China. Currently, design of pit-in-pit excavations in practice is based either on numerical simulations or on a trial and error procedure in the field. There is an urgent need to develop a simplified approach that is satisfactorily accurate and easy to be implemented for calculation of passive earth pressures in pit-in-pit excavations.

This investigation extends the initial work of Hu *et al.* [35] by introducing the correlation between the mobilized shear strength parameters of soil and the displacement ratio of retaining wall. The contribution of soil cohesion is converted into an equivalent friction angle. A trapezoidal-shaped failure wedge is formed between two parallel walls, which is divided into a rectangular zone and a triangular zone. The current analysis adopts the same assumption of Hu *et al.* [35] for the soil in the rectangular zone, where a complete symmetric arch is mobilized with the base acting on two walls. For the triangular zone, a half arch is proposed with one base acting on the 1st level retaining wall and another base acting on the inclined shear surface. The method enables to analyze the mobilized passive earth pressure for both cohesionless and cohesive soils at any intermediate state. A parametric study is carried out to demonstrate that the mobilized passive earth pressure increases with the magnitude of wall movement and soil shear strength parameters. A design chart is produced to calculate the allowable spacing between two walls. Experimentally measured earth pressures for pit-in-pit excavations from the model-scale tests of Zheng *et al.* [10] are compared with the proposed analytical model. It is found that the proposed method reproduces the trends in measurements much better than the conventional Coulomb and Rankine theories.

Last, it is reminded that the proposed analytical model in this paper is based on the assumption of one homogeneous soil layer for the pit excavation. For cases where the soil profile consists of multiple layers, the method of equating the multi-layer soil profile into an equivalent one-layer soil profile can be adopted. Nevertheless, this would bring extra uncertainty to the existing model error and should only be implemented with cautions. For cases with very complicated site conditions, more advanced modelling and analysis tools should be employed. Then the analysis outcomes using the present analytical model can be used to perform a general cross check of the design.

LIST OF NOTATIONS

c = Soil cohesion
c_m = Mobilized soil cohesion
c_w = Apparent soil cohesion
H = embedded depth of the 1st retaining wall
H_1 = Excavation height of the 2nd retaining wall
H_m = Excavation height of the 1st retaining wall
H' = Depth of the failure wedge plane
K = Lateral earth pressure coefficient
K_p = Rankine lateral earth pressure coefficient
K_0 = K_p at initial passive state
K_{wp} = K_p for cohesionless soils
K_{wpm} = K_{wp} at intermediate state
K'_{wp} = K_p for cohesive soils
K'_{wpm} = K'_{wp} at intermediate state
R = Radius of soil arch
S = Spacing of the 1st and 2nd retaining walls
β = Inclination angle of failure wedge
ϕ = Soil friction angle
ϕ_0 = ϕ at initial passive state
ϕ_d = Equivalent soil friction angle
ϕ_m = Soil friction angle at intermediate passive state
δ = Soil-wall interface friction angle
δ_0 = δ at initial passive state
δ_m = δ at intermediate passive state
θ = Soil arching rotation angle
θ_m = θ at intermediate passive state
γ = Soil unit weight
η = Percentage of full wall movement
μ = Interface friction coefficient
σ_1 = The first major principle stress
σ_3 = The third major principle stress
σ_h = Horizontal stress
σ_{mh} = Horizontal stress at an arbitrary point
σ_{av} = Average vertical stress
σ_v = Vertical stress
σ_{mv} = Vertical stress at an arbitrary point
σ' = Normal stress in the shifted coordinate system
τ_w = Shear stress
τ' = Shear stress in the shifted coordinate system
ψ = Angle of major principle stress to the horizontal

REFERENCES

[1] T. S. O'Neal and D. J. Hagerty, "Earth pressures in confined cohesionless backfill against tall rigid walls—A case history," *Can. Geotech. J.*, vol. 48, no. 8, pp. 1188–1197, 2011.
[2] M. Son, "Earth pressure on the support system in jointed rock mass," *Can. Geotech. J.*, vol. 50, no. 5, pp. 493–502, 2013.
[3] G. Zheng, Y. Guo, D. Nie, Y. Diao, and C. Liu, "Theory of multi-bench retaining for large area foundation pit and its engineering application," *Rock Soil Mech.*, vol. 35, no. S2, pp. 290–298, 2014.
[4] X. Zhang, J. Yang, Y. Zhang, and Y. Gao, "Cause investigation of damages in existing building adjacent to foundation pit in construction," *Eng. Failure Anal.*, vol. 83, pp. 117–124, Jan. 2018.

[5] S. Frydman and I. Keissar, "Earth pressure on retaining walls near rock faces," *J. Geotech. Eng.*, vol. 113, no. 6, pp. 586–599, 1987.
[6] W. A. Take and A. J. Valsangkar, "Earth pressures on unyielding retaining walls of narrow backfill width," *Can. Geotech. J.*, vol. 38, no. 6, pp. 1220–1230, 2001.
[7] Y. Hong and C. W. W. Ng, "Base stability of multi-propped excavations in soft clay subjected to hydraulic uplift," *Can. Geotech. J.*, vol. 50, no. 2, pp. 153–164, 2013.
[8] Y.-S. Fang, T.-J. Chen, and B.-F. Wu, "Passive earth pressures with various wall movements," *J. Geotech. Eng.*, vol. 120, no. 8, pp. 1307–1323, 1994.
[9] Y.-S. Fang, Y.-C. Ho, and T.-J. Chen, "Passive earth pressure with critical state concept," *J. Geotech. Geoenviron. Eng.*, vol. 128, no. 8, pp. 651–659, 2002.
[10] G. Zheng, D. Nie, X. Cheng, Y. Diao, and J. Liu, "Experimental study on multi-bench retaining foundation pit," *Chin. J. Geotech. Eng.*, vol. 39, no. 5, pp. 784–794, 2017.
[11] S. Benmebarek, T. Khelifa, N. Benmebarek, and R. Kastner, "Numerical evaluation of 3D passive earth pressure coefficients for retaining wall subjected to translation," *Comput. Geotech.*, vol. 35, no. 1, pp. 47–60, 2008.
[12] K.-H. Yang and C.-N. Liu, "Finite element analysis of earth pressures for narrow retaining walls," *J. GeoEng.*, vol. 2, no. 2, pp. 43–52, 2007.
[13] G. Zheng, D.-Q. Nie, Y. Diao, and X.-S. Cheng, "Failure mechanism of multi-bench retained foundation pit," *Rock Soil Mech.*, vol. 38, no. S1, pp. 313–322, 2017.
[14] R. L. Handy, "The arch in soil arching," *J. Geotech. Eng.*, vol. 111, no. 3, pp. 302–318, 1985.
[15] J. Hou, "Study on earth pressure on retaining walls on the basis of soil arching effect," M.S. thesis, College Civil Eng. Archit., Zhejiang Univ., Hangzhou, China, 2012.
[16] X. Qin, P. Ni, and M. Zhou, "Improved analytical solution of vertical pressure on top of induced trench rigid culverts," *Geosynth. Int.*, vol. 24, no. 6, pp. 615–624, 2017.
[17] L. Li, J.-S. Dubé, and M. Aubertin, "An extension of Marston's solution for the stresses in backfilled trenches with inclined walls," *Geotech. Geolog. Eng.*, vol. 31, no. 4, pp. 1027–1039, 2013.
[18] M. H. Khosravi, T. Pipatpongsa, and J. Takemura, "Theoretical analysis of earth pressure against rigid retaining walls under translation mode," *Soils Found.*, vol. 56, no. 4, pp. 664–675, 2016.
[19] X. Ji, P. Ni, M. Barla, W. Zhao, and G. Mei, "Earth pressure on shield excavation face for pipe jacking considering arching effect," *Tunnelling Underground Space Technol.*, vol. 72, pp. 17–27, Feb. 2018.
[20] M. Luan and T. Nogami, "Variational analysis of earth pressure on a rigid earth-retaining wall," *J. Eng. Mech.*, vol. 123, no. 5, pp. 524–530, 1997.
[21] D.-Y. Zhu and Q. Qian, "Determination of passive earth pressure coefficients by the method of triangular slices," *Can. Geotech. J.*, vol. 37, no. 2, pp. 485–491, 2000.
[22] J. M. Duncan and R. L. Mokwa, "Passive earth pressures: Theories and tests," *J. Geotech. Geoenviron. Eng.*, vol. 127, no. 3, pp. 248–257, 2001.
[23] S.-Q. Peng, J. Zhou, L. Fan, and A.-H. Liu, "Research on earth pressure of rigid retaining wall considering soil arching," *Rock Soil Mech.*, vol. 29, no. 10, pp. 2701–2707, 2008.
[24] T. Vo and A. R. Russell, "Interaction between retaining walls and unsaturated soils in experiments and using slip line theory," *J. Eng. Mech.*, vol. 143, no. 4, p. 04016120, 2016.
[25] G. Mei, Q. Chen, and L. Song, "Model for predicting displacement-dependent lateral earth pressure," *Can. Geotech. J.*, vol. 46, no. 8, pp. 969–975, 2009.
[26] P. Ni, G. Mei, and Y. Zhao, "Displacement-dependent earth pressures on rigid retaining walls with compressible geofoam inclusions: Physical modeling and analytical solutions," *Int. J. Geomech.*, vol. 17, no. 6, p. 04016132, 2017.
[27] P. Ni, S. Mangalathu, L. Song, G. Mei, and Y. Zhao, "Displacement-dependent lateral earth pressure models," *J. Eng. Mech.*, vol. 144, no. 6, p. 04018032, 2018.
[28] P. Ni, L. Song, G. Mei, and Y. Zhao, "On predicting displacement-dependent earth pressure for laterally loaded piles," *Soils Found.*, vol. 58, no. 1, pp. 85–96, 2018.
[29] A. Keshavarz and M. Ebrahimi, "Axisymmetric passive lateral earth pressure of retaining walls," *KSCE J. Civil Eng.*, vol. 21, no. 5, pp. 1706–1716, 2017.
[30] Y. Sun, S. Zhou, and Z. Luo, "Basal-heave analysis of pit-in-pit braced excavations in soft clays," *Comput. Geotech.*, vol. 81, pp. 294–306, Jan. 2017.
[31] C. Xiong, Q. Min, and J. Wang, "Analysis of the bar system FEM of pit in pit excavation," *J. Eng. Geol.*, vol. 20, no. S1, pp. 787–792, 2012.
[32] M. Yang, J. Zhang, and R. Wang, "Analysis of internal force of deformation of retaining wall in pits-in-pits," *Rock Soil Mech.*, vol. 37, no. 11, pp. 3270–3274, 2016.
[33] M. Saiyar, P. Ni, W. A. Take, and I. D. Moore, "Response of pipelines of differing flexural stiffness to normal faulting," *Géotechnique*, vol. 66, no. 4, pp. 275–286, 2016.
[34] A. W. Storey, "Design optimization of safety benches for surface quarries through rockfall testing and evaluation," M.S thesis, Dept. Mining Minerals Eng., Virginia Polytech. Inst. State Univ., Blacksburg, VA, USA, 2010.
[35] H. Hu, L. Tang, X. Lin, and H. Sang, "Analysis of soil arching effects in pit-in-pit passive zone as supporting structure parallel movement," *Acta Scientiarum Naturalium Universitatis Sunyatseni*, vol. 53, no. 1, pp. 135–140, 2014.
[36] G. W. Clough and J. M. Duncan, "Earth pressures," in *Foundation Engineering Handbook* (Van Nostrand Reinhold), H.-Y. Fang, Ed., 2nd ed. New York, NY, USA: Springer, 1991, pp. 223–235.
[37] D. E. Becker and I. D. Moore, *Canadian Foundation Engineering Manual*, C. G. Society, Ed. Richmond, BC, Canada: Alliston, 2006.
[38] J. G. Potyondy, "Skin friction between various soils and construction materials," *Géotechnique*, vol. 11, no. 4, pp. 339–353, 1961.

HUI HU received the Ph.D. degree in engineering mechanics from the School of Earth Science and Engineering, Sun Yat-sen University, China, in 2013. He is currently a Senior Engineer and an Associate Professor with the School of Mechanics and Construction Engineering, Jinan University, Guangzhou, China. His research interests include geomaterial constitute modeling, soil and foundation engineering, and geotechnical structure monitoring techniques.

MENGQI YANG received the Ph.D. degree in geography from the Department of Geography and Planning, Queen's University, Canada, in 2018. She is currently a Postdoctoral Fellow with Guangzhou University, China.

PEIYUAN LIN received the Ph.D. degree in civil engineering from the Department of Civil Engineering, Ryerson University, Canada, in 2016. He is currently a Postdoctoral Research Fellow with Ryerson University. His research interests include reliability-based design of geotechnical structures, geotechnical risk, infrastructure deterioration modeling, stochastic modeling, and infrastructure asset management.

XINGLI LIN received the M.A.Sc. degree in civil engineering from the School of Mechanics and Construction Engineering, Jinan University, China, in 2017. He is currently a Junior Engineer with a geotechnical consultant company in China.